AGU PUBLICATIONS

Geophysical Research Letters

RESEARCH LETTER
10.1002/2014GL061142

**Key Points:**
- First coupled simulation from GrIS model and AOGCM under RCP/ECP forcing
- Surface mass balance, elevation, and ice flow are strongly coupled
- Ensemble reveals wide spread in simulated present-day mass trends

**Supporting Information:**
- Texts S1 and S2, Figures S1–S7, and Table S1

**Correspondence to:**
M. Vizcaino,
M.Vizcaino@tudelft.nl

**Citation:**
Vizcaino, M., U. Mikolajewicz, F. Ziemen, C. B. Rodehacke, R. Greve, and M. R. van den Broeke (2015), Coupled simulations of Greenland Ice Sheet and climate change up to A.D. 2300, *Geophys. Res. Lett.*, *42*, 3927–3935, doi:10.1002/2014GL061142.

Received 19 FEB 2015
Accepted 21 APR 2015
Accepted article online 23 APR 2015
Published online 19 MAY 2015



# Coupled simulations of Greenland Ice Sheet and climate change up to A.D. 2300

**Miren Vizcaino[1], Uwe Mikolajewicz[2], Florian Ziemen[2,3], Christian B. Rodehacke[2,4], Ralf Greve[5], and Michiel R. van den Broeke[6]**

[1]Department of Geoscience and Remote Sensing, Delft University of Technology, Delft, Netherlands, [2]Max Planck Institute for Meteorology, Hamburg, Germany, [3]Geophysical Institute, University of Alaska, Fairbanks, Alaska, United States, [4]Now at Department of Arctic and Climate Research, Danish Meteorological Institute, Copenhagen, Denmark, [5]Institute of Low Temperature Science, Hokkaido University, Sapporo, Japan, [6]Institute for Marine and Atmospheric Research, Utrecht University, Utrecht, Netherlands

**Abstract** Recent observations indicate a high sensitivity of the Greenland Ice Sheet (GrIS) to climate change. We examine the coupling between the GrIS surface mass balance, elevation, and dynamical flow with one of the few coupled GrIS and atmosphere-ocean general circulation models. Bidirectional coupling from the early Holocene reveals a growing present-day GrIS in the absence of anthropogenic forcing. We identify atmospheric sources of biases in the simulated present-day GrIS and assess the GrIS sensitivity to future greenhouse gas forcing through three Representative Concentration Pathways and their extensions and to climate variability. The elevation-surface mass balance feedback contributes to future GrIS mass loss with 8–11% (by 2100), depending on the forcing scenario, and 24–31% (by 2300). Climate variability causes a 2.5 times spread in the magnitude of the simulated present-day GrIS mass trends in a three-member ensemble. Our results represent a first step toward more advanced higher resolution coupled modeling of GrIS and climate evolution.

## 1. Introduction

Remote sensing measurements indicate that the Greenland Ice Sheet (GrIS) is losing mass at an accelerating rate [*Rignot et al*., 2011; *Shepherd et al*., 2012] due to enhanced runoff and ice discharge to the ocean [*Enderlin et al*., 2014]. It is not yet clear whether current mass loss trends will be sustained or further increase into the future or what the relative contributions of anthropogenic climate change and natural climate variability are to these trends [*Bamber and Aspinall*, 2013]. Due to its limited length, the observational record cannot yet provide an answer to these questions [*Wouters et al*., 2013]. Coupled modeling of global climate with GrIS surface and ice flow processes can potentially be used instead. However, such a coupling is very challenging, owing to limited spatial model resolution, climate model biases, insufficient representation of surface processes, and lack of key observational data (e.g., ice basal conditions) [*Vizcaino*, 2014]. A few studies have used bidirectional coupled ice sheet and atmosphere-ocean general circulation models (AOGCMs) [*Ridley et al*., 2005; *Vizcaino et al*., 2008; *Vizcaíno et al*., 2010]. The majority of studies applied off-line forcing of ice sheet models using output from climate models [*Greve and Herzfeld*, 2013; *Bindschadler et al*., 2013; *Goelzer et al*., 2013; *Adalgeirsdottir et al*., 2014]. In such studies, the surface mass balance (SMB), the difference between snowfall, runoff, and sublimation, is either prescribed from a regional climate model or calculated using temperature-index models for surface melt (e.g., degree-day models, [*Reeh*, 1991]). In the former case, the ice sheet topography is kept constant for the SMB calculation, and elevation-SMB feedback are not accounted for. Temperature-index models, while accommodating changes in elevation, are not physically based and therefore are not universally applicable to different climate regimes and geographical locations [*Bougamont et al*., 2007; *Robinson et al*., 2011]. Furthermore, GCM biases in SMB fields prevent ice sheet modelers from using the atmospheric forcing directly; instead, anomaly forcing is used (e.g., *Adalgeirsdottir et al*. [2014]), which distorts feedback representation.

This study examines coupled processes of ice sheet and climate evolution up to year 2300, with special focus on the relevance of the elevation-SMB feedback for future GrIS evolution. We use a 3-D ice sheet model (ISM) with the shallow ice approximation (SIA) that is bidirectionally coupled to a coarse resolution AOGCM. The initialization procedure accounts for the present-day secular mass trend of the GrIS in response to past

climate forcing and avoids spurious background trends from nonequilibrated present-day ice and climate components. The sensitivity to greenhouse forcing and internal climate variability are assessed with three Representative Concentration Pathways (RCPs) and their extensions (Extended Concentration Pathways (ECPs)) and a three-member model ensemble for the historical and high-emission scenarios. The novelty of our approach lies in the continuous coupled simulation from the early Holocene, the relatively high number of simulations, the absence of unphysical corrections in the initialization method, and a semiexplicit SMB calculation based on the surface energy budget. Our results must be interpreted as a first step toward fully coupled higher resolution simulations with more advanced physics (e.g., less approximations in the ISM). This is why as opposed to previous uncoupled work using assimilation methods, this study focuses on the gain of incorporating the coupled processes and less on exactly reproducing the observed GrIS.

## 2. Method

We use a coarse resolution version of the AOGCM European Centre/Hamburg 5.2 (ECHAM5.2)/Max Planck Institute ocean model (MPI-OM). The horizontal resolution and vertical resolutions are, respectively, ~3.75° and 19 levels for the atmospheric component, and for the ocean model ~3° with one pole over Greenland resulting in a resolution of 30–75 km around Greenland, and 40 levels for the ocean. The model is coupled to the vegetation model Lund-Potsdam-Jena (~3.75° resolution) and the 3-D thermomechanical ISM SICOPOLIS3.0 [*Greve*, 1997], at 10 km horizontal resolution. A previous model version was used with idealized greenhouse gas forcing [*Mikolajewicz et al*., 2007b; *Vizcaíno et al*., 2010]. The main improvements in this study are the much enhanced resolution of the ISM, full climate/ice sheet coupling since 9000 B.P. for the spin-up, improved sea ice parameterizations resulting in a more realistic Arctic sea ice, and interactive calculation of the subgrid topography parameters used in the gravity wave drag parameterization [*Ziemen et al*., 2014]. In addition, the surface albedo in partially glacier-covered cells is calculated as a weighted average between the glacier albedo and the albedo of bare soil. SICOPOLIS3.0 uses the SIA, which is appropriate for large-scale ice flow but does not accurately reproduce fast-flowing outlet glaciers (see *Schoof and Hewitt* [2013] for a review on ISM approximations). Ice is immediately removed from the GrIS once it reaches the ocean. Isostatic rebound is calculated with a column model [*Le Meur and Huybrechts*, 1998]. With a 1 year coupling time step, the ISM delivers annual mean freshwater fluxes to the ocean model and an updated upscaled GrIS topography and glacier mask to the atmosphere model. The SMB is calculated as accumulation minus runoff and sublimation. Surface melt is calculated from the surface energy balance. Details on the SMB are given in the supporting information.

Three different periods are distinguished for ISM initialization. For 130,000 until 9,000 B.P., the ISM is forced with temperature and precipitation time slices from ECHAM5/MPI-OM at 21,000 B.P. and preindustrial, index weighted with the Greenland Ice Core Project temperature record [*Dansgaard et al*., 1993; *Johnsen et al*., 1997]. Surface melt is calculated with a degree-day scheme [*Greve et al*., 2011]. Between 9000 B.P. and 1500 A.D. (or 450 B.P.), the ISM is coupled to the climate model via the energy balance scheme described above using periodically synchronous coupling [*Mikolajewicz et al*., 2007a], with an acceleration factor slowly reduced from 30 to 1 during the course of the spin-up. From 1500 A.D. onward, the model was run without acceleration in the ice sheet model. Atmospheric greenhouse gas concentrations of $CO_2$, $CH_4$, and $N_2O$ were set to 280 ppmv, 350 ppbv, and 200 ppbv, respectively, between 9000 B.P. and 0 A.D.. Between 0 A.D. and 1849 A.D., they follow *Meure et al*. [2006].

The control simulation is run from year 1850 to 2300. It keeps atmospheric greenhouse gas concentrations ($CO_2$: 285 ppmv, $CH_4$: 791 ppbv, and $N_2O$: 275 ppbv) and insolation at 1850 values. None of the runs include volcanic eruptions or variations in the solar constant as forcing. A simulation with historical greenhouse gases is run between 1850 and 2000, while three RCP/ECPs are used from 2000 to 2300 [*van Vuuren et al*., 2011]: RCP-ECP2.6, RCP-ECP4.5, and a modified RCP-ECP8.5, where the atmospheric $CO_2$ concentration ($pCO_2$) reaches values of 421, 538, and 936 ppmv by year 2100, respectively (Figure 1a). In RCP2.6, the $pCO_2$ increases up to year 2040 and decreases afterward. In RCP4.5, it equilibrates shortly after 2100. The original $pCO_2$ from RCP-ECP8.5 has been capped at 4 times preindustrial values and is denoted RCP-ECP8.5_4x. To quantify internal climate variability, three ensemble simulations for the period of 1850–2300 with identical solar and greenhouse (historical and RCP-ECP8.5_4x scenarios) forcings were

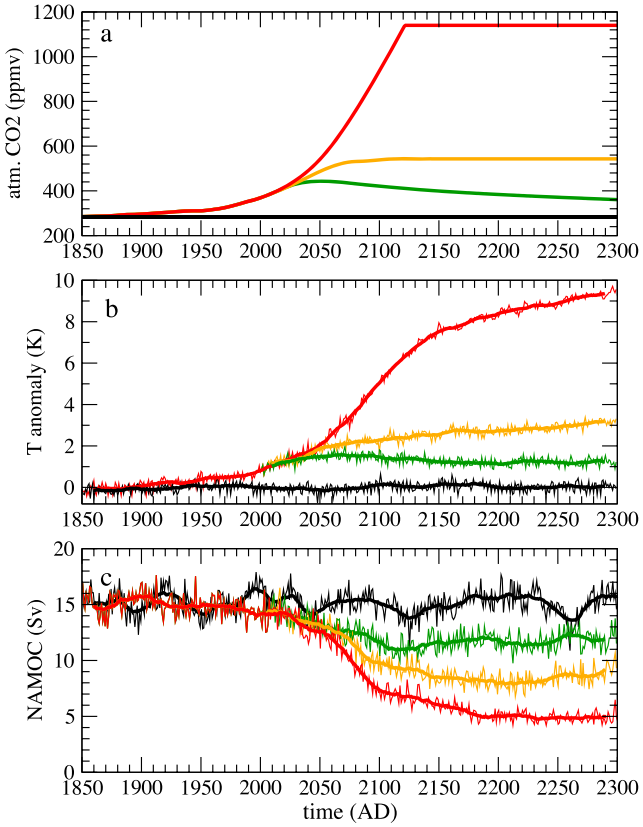


**Figure 1.** Annual and 20 year mean (thick) time series for preindustrial control (black), historical (red), RCP-ECP2.6 (green), RCP-ECP4.5 (orange), and RCP-ECP8.5_4x (red): (a) global atmospheric $CO_2$ concentration (ppmv), (b) anomalies of global mean near-surface air temperatures relative to the control 1850–2300 mean (K), and (c) maximum NAMOC strength (sverdrup).

started from the model states reached in three different years (1699, 1799, and 1849 A.D.) of the spin-up simulation.

In order to evaluate the effect of ice sheet elevation change on the SMB, three additional off-line simulations—one per scenario—have been performed. In each of them, the SMB is calculated with the same atmospheric model output as in the reference coupled simulation, at a fixed (1980–1999 mean) ISM elevation. The ISM is permitted to evolve freely. The elevation-SMB feedback is quantified by differencing the fully coupled and off-line runs. This approach does not account explicitly for the effect of a changing topography on the large-scale atmospheric circulation of the AOGCM. Up to 2300, the topography change at the AOGCM resolution is small and does not significantly impact the simulated GrIS evolution [*Ridley et al.*, 2005; *Vizcaino et al.*, 2008; *Vizcaíno et al.*, 2010]. Explicit modeling of the impacts of GrIS elevation changes on the regional atmospheric circulation for the 1850 A.D.–2300 A.D. period would require a much higher resolution (on the order of tens of kilometers or below) in the atmospheric model.

## 3. Holocene Evolution and Present-Day Ice Sheet

In response to high summer insolation during the early and mid-Holocene, the GrIS loses mass from an initial 8.8 m sea level equivalent (SLE) (Figure S1 in the supporting information) at 9000 B.P. to a 7.7 m SLE minimum at ~3500 B.P., which represents ~0.20 mm $yr^{-1}$ of sea level rise (SLR) during this period. From ~3500 B.P., the GrIS slowly grows by ~0.04 mm SLE $yr^{-1}$, reaching 7.9 m SLE by 1850 A.D.. In the absence of anthropogenic forcing (control run), the GrIS gains mass during the 1850–2000 period, equivalent to −7 mm SLR. In the 1850–2000 historical simulation, the GrIS gains mass as well, −2 mm SLR. This implies that the 1850–2000 net effect of anthropogenic greenhouse gas emissions is +5 mm SLR.

The present-day (mean 1960–2005) simulated GrIS has an area and a volume of $1.978 \cdot 10^6$ $km^2$ and 7.9 m SLE, respectively, which exceed observations by $0.27 \cdot 10^6$ $km^2$ and 0.5 m SLE [*Bamber et al.*, 2013]. For most of Greenland, the limits of the modeled GrIS extend beyond observations, while the simulated northwest margin is up to some hundreds of kilometers too far from the coast (Figure S2 in the supporting information). The modeled ice sheet is too thick in relatively dry areas, i.e., the northern, eastern, and southwestern margins, and too thin in wet areas, i.e., the northwest and southeast [*Ettema et al.*, 2009], and in the central northeast. The simulated GrIS extends over areas that currently are covered by isolated ice caps (e.g., northern Greenland). These thickness biases are mostly related to biases in the SMB simulation, which are discussed in the next paragraph. The biases could be artificially corrected [e.g., *Adalgeirsdottir et al.*, 2014] or avoided with a different initialization method involving assimilation of topography and/or ice flow data [e.g., *Price et al.*, 2011]. However, our target in this work is to maintain the influence of multicentury memory and to avoid spurious trends that result from artificially imposing

optimized forcings. This is consistent with the technique for AOGCM projections, which are also initialized from a long coupled spin-up and not from an ocean state consistent with observations.

Comparison of GrIS SMB calculated at the present-day observed elevation with results from the regional climate model Regional Atmospheric Climate Model version 2 (RACMO2) [*van Angelen et al*., 2012] (Figure S3 in the supporting information) shows reasonable distributions of the ablation (SMB $< 0$) and accumulation (SMB $> 0$) areas, with major biases attributable to the difference in the resolution of the atmosphere model. The best match between the positions of the equilibrium line (SMB $= 0$) is found over the northern and northwestern margins. Accumulation rates are overestimated over the northern half of the ice sheet, and observational regional maxima in the northwest and southwest are underestimated, due to reduced orographic forcing in our low-resolution model. The low resolution and the absence of coupling between snowfall and surface albedo in our model may also explain south to north SMB differences along the western margin. The simulated ablation areas over the simulated model topography (Figure S3 in the supporting information (top)) have similar widths compared to RACMO2, except for a too wide ablation area in the southeast, where higher accumulation rates in RACMO2 prevent net loss at the surface.

The three historical simulations show negative mass trends over the period of 1990–2013 (Figure S4 in the supporting information): 0.06, 0.08, and 0.15 mm $yr^{-1}$ SLR. The large variability between these numbers suggest a significant role of natural climate variability (mainly related to the large-scale circulation) on the current mass loss trends, in line with *Fettweis et al*. [2013]. Our estimates are a factor 2.5–5 smaller than the reconciled 1992–2011 mass loss ($0.39 \pm 0.13$ mm $yr^{-1}$) [*Shepherd et al*., 2012]. The main sources of this underestimation of modern mass loss is that our simulations do not account for the recently observed acceleration of outlet glaciers (e.g., *Moon et al*. [2012]), which is considered to be primarily driven by ocean forcing [*Joughin et al*., 2012], and that our model underestimates the melt-albedo feedback, maintaining high albedo values (0.55) for bare ice. This discrepancy must be kept in mind when interpreting the model projections in the following section.

## 4. The 2000 to 2300 Ice Sheet Mass Change and Contributions From Surface and Ice Flow Processes

The modeled annual global mean near-surface air temperature increase by year 2080–2099 with respect to the preindustrial mean is 1.5 K (RCP2.6), 2.2 K (RCP4.5), and 4.3 K (RCP8.5) (Figure 1b). The warming intensifies beyond 2100 in ECP4.5 and ECP8.5_4x, but reverses under ECP2.6, with temperature anomalies being 1.2, 3.2, and 9.4 K by 2280–2299. For all simulations, warming is reduced in the North Atlantic region as a result of a weakened North Atlantic Meridional Overturning Circulation (NAMOC) (Figure 1c).

The GrIS volume change at year 2100 with respect to year 2000 is equivalent to 27 mm (RCP2.6), 34 mm (RCP4.5), and 58 mm (RCP8.5) of global mean SLR (Figure 2a). In order to compare the GrIS change with its "unforced" evolution (control run), 10 mm SLR should be added (5 mm from the control and historical differences during 1850–2000 and 5 mm for the sustained mass gain between A.D. 2000 and 2100 in the control run), resulting in 37, 44, and 68 mm SLR with respect to the nonanthropogenic-forced GrIS. The total sea level contributions that can be attributed to anthropogenic greenhouse forcing by A.D. 2300 are 68, 135, and 539 mm. The simulated GrIS evolution varies much less among the three-ensemble simulations (Figure S4 in the supporting information) than among simulations with different greenhouse gas scenarios: the mean and standard deviations ($\sigma$) for the three RCP-ECP8.5_4x simulations are 67 and 1 mm by 2100 and 536 and 7 mm by 2300. This suggests a linear increase of $\sigma$ with the mean.

### 4.1. SMB Change

The GrIS-integrated SMB decreases in all projections (Table 1 and Figure 2b), becoming negative by the end of the 21st century under RCP4.5 and RCP8.5 forcing. Total accumulation rates (snowfall minus sublimation) increase by 7% (RCP4.5), 9% (RCP4.5), and 18% (RCP8.5), in connection with an enhanced global hydrological cycle. Runoff increases (60%, 84%, and 273%), however, largely exceed accumulation increases, leading to net surface mass loss. Between 2100 and 2300, the SMB evolution is very different across the ECP runs. By A.D. 2300, the RCP-ECP2.6 SMB increases with respect to 2100, with a small

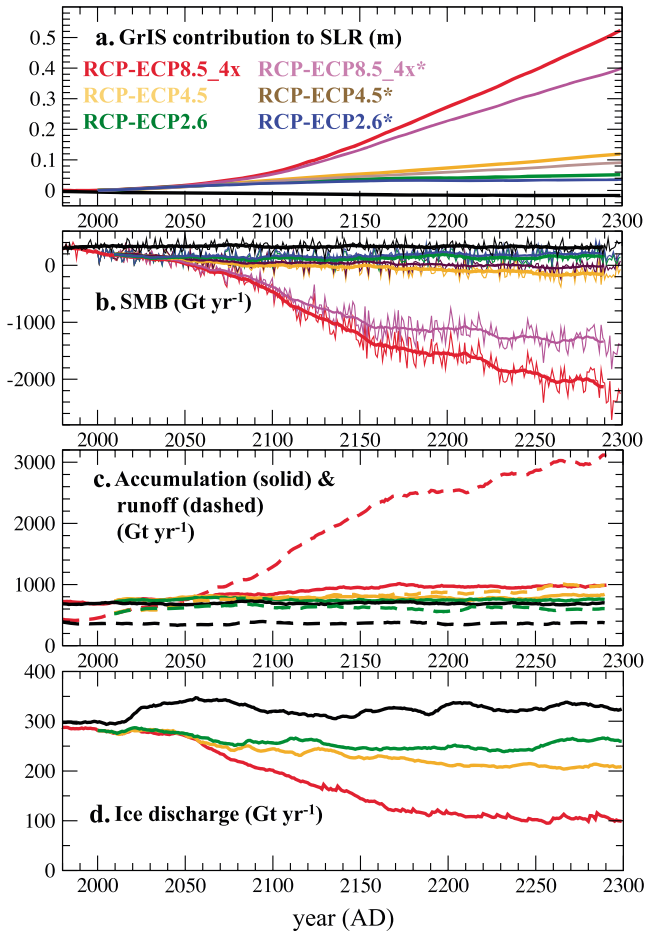


**Figure 2.** (a) GrIS contribution to sea level rise (m) with respect to A.D. 2000 for the preindustrial control (black), RCP-ECP2.6 (green, *blue), RCP-ECP4.5 (orange, *maroon), and RCP-ECP8.5_4x (red, *magenta) simulations. The * simulations do not include the elevation-SMB feedback. (b) Area-integrated SMB and 20 year running means (thick). (c) The 20 year running means of accumulation (snowfall minus sublimation, solid) and runoff (dashed). (d) Ice discharge to the ocean. The units in Figures 2b–2d are Gt $yr^{-1}$.

decrease in accumulation rates and much reduced runoff rates, but it remains well below 2000 levels. In RCP-ECP4.5, accumulation and runoff continue to increase, with runoff in 2300 being 235% of the 1980–2000 mean value. In RCP-ECP8.5_4x, runoff increases sevenfold in 2300 with respect to the 1980–1999 value. The SMB interannual variability increases in all simulations, as in results from a different model [*Fyke et al.*, 2014].

The equilibrium line altitude increases in all simulations (Figure S5 in the supporting information), particularly in the northern half of the ice sheet, in connection with maximum sensitivity to sea ice retreat, as in *Ridley et al.* [2005] and *Vizcaino et al.* [2013]. However, the strong reduction of the high northern accumulation areas in RCP-ECP8.5_4x is not found in other studies. This reduction is likely due to positive temperature bias caused by the too low topography at the course resolution of the atmospheric model. The SMB increases over the accumulation area in the north and southwest due to enhanced snowfall (Table 1).

### 4.2. Elevation Change

Elevation changes are the result of combined changes in the cumulative SMB and in ice dynamics. We examine their relative contributions for the end of the 21st century in the most extreme scenario RCP8.5 (Figure S6 and Table S1 in the supporting information). Increased melt in the low-lying areas of the ice sheet and subsequent expansion of the ablation area cause high negative cumulative SMB anomalies in the lowest parts of the ice sheet. At higher elevations, anomalies are generally positive but of smaller magnitude. As a result, the elevation gradient (slope) in the ice sheet surface increases, enhancing ice flow from the interior to the margins. Spatially, the cumulative SMB anomalies range from −660 m to 32 m, averaging −16 m (Table S1 in the supporting information). While the general pattern of elevation change is similar to the cumulative SMB anomalies, important differences occur along the SE and southern margins, where the cumulative SMB gradients are highest due to both higher accumulation and melt rates in these areas and to the high topographic gradient. These differences follow from enhanced ice flow driven by the increased surface slope. This enhanced ice transport partly counterbalances the strong losses by surface melt, as shown in previous work [*Edwards et al.*, 2014; *Adalgeirsdottir et al.*, 2014; *Huybrechts and de Wolde*, 1999; *Vizcaino et al.*, 2008]. Spatially, the ice flow contribution ranges from −313 to 478 m, with a positive mean value of 4 m. The more negative elevation anomalies are dominated by the SMB contribution (Figure S6d in the supporting information), while the ice flow contribution dominates over accumulation areas close to the equilibrium line (Figures S5, S6b, and S6d in the supporting information).

**Table 1.** Mean and Standard Deviation of Mass Balance Components[a] in the Historical and Scenario Runs[b] (Gt yr$^{-1}$)

| | Historical 1980–1999 | RCP2.6 2080–2099 | RCP-ECP2.6 2280–2299 | RCP4.5 2080–2099 | RCP-ECP4.5 2280–2299 | RCP8.5 2080–2099 | RCP-ECP8.5_4x 2280–2299 |
|---|---|---|---|---|---|---|---|
| SMB | 288 ± 65 | 88 ± 83 (16%) | 149 ± 97 (39%) | −5 ± 80 (14%) | −145 ± 103 (31%) | −313 ± 102 (11%) | −2132 ± 255 (33%) |
| Acc | 707 ± 62 | 760 ± 72 (−2%) | 756 ± 49 (−4%) | 768 ± 74 (−3%) | 840 ± 108 (−5%) | 832 ± 70 (−3%) | 991 ± 62 (−14%) |
| RU | 419 ± 50 | 671 ± 65 | 606 ± 67 | 773 ± 69 | 986 ± 83 | 1145 ± 76 | 3124 ± 244 |
| D | 286 ± 1 | 257 ± 2 | 263 ± 2 | 245 ± 3 | 210 ± 2 | 209 ± 6 | 105 ± 5 |

[a]SMB = surface mass balance, Acc = accumulation, RU = runoff, and D = ice discharge to the ocean.
[b]The relative contributions of the elevation-SMB and elevation-precipitation feedback are indicated in parentheses.

### 4.3. Elevation-SMB Feedback

The elevation-SMB feedback is examined by comparing each scenario simulation to a corresponding sensitivity simulation, where the SMB is calculated at the modeled 1980–1999 ISM topography ("*" simulations in Figure 2). The elevation-SMB feedback increases the total mass loss in all simulations, acting as a positive feedback. By A. D. 2100, the relative contribution to SLR is 11% (RCP2.6), 10% (RCP4.5), and 8% (RCP8.5). In terms of SMB change, the relative contributions are higher, 16%, 14%, and 11%, respectively (Table 1), which indicates greater relative importance in the moderate scenarios. By 2300, due to further elevation changes, the additional volume loss increases to 31%, 24%, and 24%; i.e., the relative SLR contribution almost triples.

When evaluating the elevation-SMB feedback, the contributions from accumulation and ablation should be considered separately. First, elevation change may cause precipitation change due to the elevation-desertification effect. Second, elevation change may modify the snowfall-to-rain ratio as a result of elevation-induced temperature change. Third, elevation changes modify runoff rates due to changed near-surface atmospheric conditions (e.g., incoming radiation and temperature). The latter is the dominant process in our simulations: runoff increases at reduced elevations.

The simulated elevation changes result in negative SMB anomalies over most of the GrIS (Figure 3a), with the most negative anomalies at the margins. High positive SMB anomalies appear in areas where ice flow increases the local elevation (Figure S6 in the supporting information). Smaller positive SMB anomalies appear in parts of the accumulation area where surface runoff decreases due to increased elevations from climate-change-induced increased precipitation. Taking the ratio between SMB change associated with topographic change and the amount of elevation change as a metric to quantify it, the elevation-SMB feedback reveals large spatial gradients over the ice sheet (Figure 3b). This is consistent with *Helsen et al.* [2012], who applied a different method to compute contemporary SMB fields. The feedback is positive in the areas where the elevation-melt feedback is dominant (ablation areas, particularly at lowest elevations) and over part of the accumulation areas having significant surface melt. The feedback is negative over most of the accumulation area, where the elevation-desertification feedback is dominant. Since accumulation increases in all simulations (Table 1), this negative feedback results in negative SMB anomalies that contribute to the overall mass loss caused by SMB-elevation coupling. When integrated over the ice sheet, elevation changes reduce accumulation rates by 2–14% in all scenarios (Table 1).

### 4.4. Ice Sheet Discharge to the Ocean

Modeled ice sheet discharge decreases with time in all simulations (Table 1 and Figure 2d) except under RCP-ECP2.6 forcing between 2100 and 2300, where discharge rates slightly increase. During this period and under this scenario, global warming is reduced in 2300 with respect to 2100 (Figure 1b) and the net SMB increases (Table 1). The decrease in ice discharge is due to modeled reduction in the number of discharge locations and a decrease in the magnitude of ice discharge for individual locations. These reductions are caused by ice sheet retreat and marginal thinning caused by increased ablation (Figure S7 in the supporting information). However, the modeled present-day locations of ice sheet discharge are not realistic over large parts of the ice sheet margins, as the northwest margin, which is too far from the ocean (Figure S2 in the supporting information). In addition, the ice sheet model resolution (10 km) is larger than the observed width of most of the GrIS outlet glaciers. A future decrease in GrIS ice discharge to the oceans is also simulated in other whole GrIS studies [*Ridley et al.*, 2005; *Gillet-Chaulet et al.*, 2012; *Lipscomb et al.*, 2013]. However, a regional higher order flow line model projects increased discharge of the four major GrIS outlet glaciers [*Nick et al.*, 2013]. The latter model resolves specific bed geometry characteristics for each

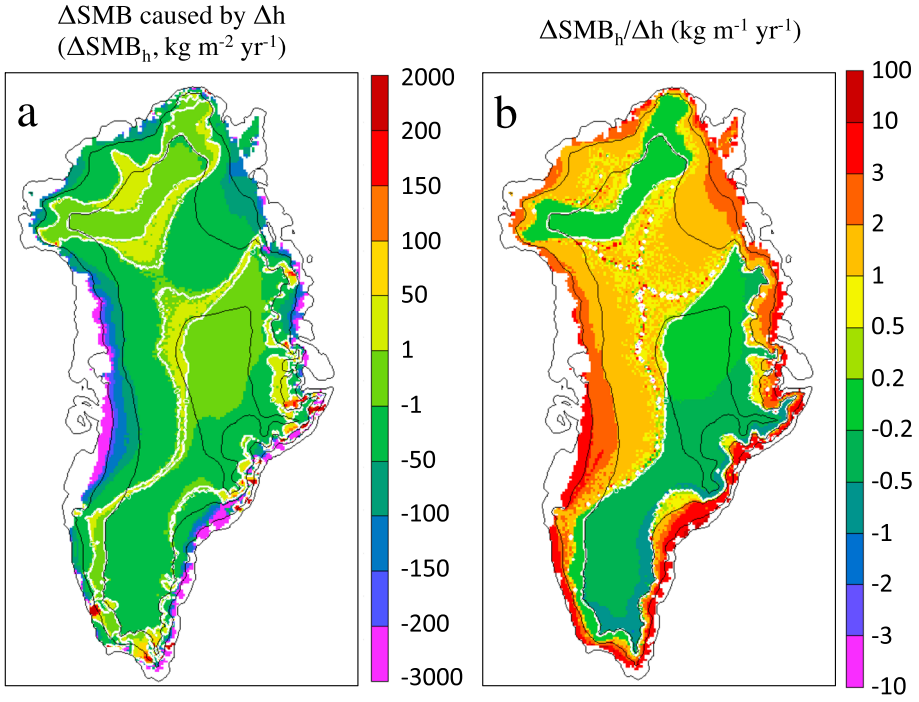


**Figure 3.** (a) The 2080–2099 SMB anomaly (kg m$^{-2}$ yr$^{-1}$) with respect to 1980–1999 associated with elevation change under RCP8.5. (b) Ratio between Figure 3a and elevation change, quantifying the elevation-SMB feedback (kg m$^{-1}$ yr$^{-1}$). The zero contours and elevation contours at 1000 m intervals are shown in white and black, respectively.

glacier and includes processes of ocean-outlet glacier interaction; however, it lacks the coupling with the whole GrIS large-scale evolution.

## 5. Conclusion and Outlook

This study explores the interactions between GrIS surface mass balance, elevation, and flow in a coupled framework that permits the examination of multicentury trends and of multiple scenarios of climate change. In the absence of anthropogenic forcing, the simulated GrIS gains mass during the 1850–2300 period, likely due to GrIS recovery following the early and mid-Holocene insolation maximum. Our results suggest an 8–11% increased mass loss of the GrIS by A.D. 2100 due to elevation-SMB feedback. This contribution increases with time, as surface elevation continues to decrease, reaching 24–31% by A.D. 2300. The feedback is dominated by the contribution of lower ablation areas, where melting increases the most and elevation changes are the largest. Our study also suggests a future decrease in ice discharge due to marginal thinning and retreat, in agreement with previous work accounting for the competition between mass loss at the surface and at the ocean interface [*Gillet-Chaulet et al.*, 2012; *Goelzer et al.*, 2013; *Lipscomb et al.*, 2013; *Edwards et al.*, 2014].

Ice sheets are a key interactive component of the Earth system, and the importance of coupling ice sheets and AOGCMs has been widely recognized [*Widmann*, 2009; *Alley and Joughin*, 2012; *Joughin et al.*, 2012; *Rae et al.*, 2012; *Hanna et al.*, 2013]. The study presented here must be regarded a necessary first step toward more advanced coupling of ice sheet and climate models at higher resolution, for instance with improved surface-atmosphere coupling (e.g., explicit representation of snow albedo evolution), less simplified ice sheet flow dynamics, and the inclusion of ocean forcing to Greenland outlet glaciers.

**Acknowledgments**
Two anonymous reviewers and the Editor Julienne Stroeve are thanked for their insightful comments. M. Vizcaino is funded via a Marie Curie International Incoming Fellowship (FP7-PEOPLE-2010-IIF-272956) and the Delft Technology Fellowship. U. Mikolajewicz acknowledges funding from THOR, a project of the European Union 7th Framework Programme (FP7 2007–2013) under grant agreement n.212643. R. Greve was supported by the Japan Society for the Promotion of Science through Grants-in-Aid for Scientific Research A (22244058 and 25241005) and by MEXT Japan through the GRENE Arctic Climate Change Research Project "Rapid Change of the Arctic Climate System and its Global Influences" (2011–2016). Simulations have been performed at the Deutsches Klimarechenzentrum through support from the German Federal Ministry of Education and Research (BMBF). Model output is available upon request.

The Editor thanks two anonymous reviewers for their assistance in evaluating this paper.

## References

Adalgeirsdottir, G., A. Aschwanden, C. Khroulev, F. Boberg, R. Mottram, P. Lucas-Picher, and J. H. Christensen (2014), Role of model initialization for projections of 21st century Greenland Ice Sheet mass loss, *J. Glaciol.*, *60*(222), 782–794, doi:10.3189/2014jog13j202.

Alley, R. B., and I. Joughin (2012), Modeling ice sheet flow, *Science*, *336*(6081), 551–552, doi:10.1126/Science.1220530.

Bamber, J. L., and W. P. Aspinall (2013), An expert judgment assessment of future sea level rise from the ice sheets, *Nat. Clim. Change*, *3*(4), 424–427, doi:10.1038/Nclimate1778.

Bamber, J. L., et al. (2013), A new bed elevation data set for Greenland, *Cryosphere*, *7*(2), 499–510, doi:10.5194/Tc-7-499-2013.
Bindschadler, R. A., et al. (2013), Ice sheet model sensitivities to environmental forcing and their use in projecting future sea level (the SeaRISE project), *J. Glaciol.*, *59*(214), 195–224, doi:10.3189/2013jog12j125.
Bougamont, M., J. L. Bamber, J. K. Ridley, R. M. Gladstone, W. Greuell, E. Hanna, A. J. Payne, and I. Rutt (2007), Impact of model physics on estimating the surface mass balance of the Greenland Ice Sheet, *Geophys. Res. Lett.*, *34*, L17501, doi:10.1029/2007GL030700.
Dansgaard, W., et al. (1993), Evidence for general instability of past climate from a 250 kyr ice core record, *Nature*, *364*(6434), 218–220.
Edwards, T. L., et al. (2014), Effect of uncertainty in surface mass balance-elevation feedback on projections of the future sea level contribution of the Greenland Ice Sheet, *Cryosphere*, *8*(1), 195–208, doi:10.5194/Tc-8-195-2014.
Enderlin, E. M., I. M. Howat, S. Jeong, M.-J. Noh, J. H. van Angelen, and M. R. van den Broeke (2014), An improved mass budget for the Greenland Ice Sheet, *Geophys. Res. Lett.*, *41*, 866–872, doi:10.1002/2013GL059010.
Ettema, J., M. R. van den Broeke, E. van Meijgaard, W. J. van de Berg, J. L. Bamber, J. E. Box, and R. C. Bales (2009), Higher surface mass balance of the Greenland Ice Sheet revealed by high-resolution climate modeling, *Geophys. Res. Lett.*, *36*, L12501, doi:10.1029/2009GL038110.
Fettweis, X., E. Hanna, C. Lang, A. Belleflamme, M. Erpicum, and H. Gallee (2013), Important role of the midtropospheric atmospheric circulation in the recent surface melt increase over the Greenland Ice Sheet, *Cryosphere*, *7*(1), 241–248, doi:10.5194/Tc-7-241-2013.
Fyke, J. G., M. Vizcaíno, W. Lipscomb, and S. Price (2014), Future climate warming increases Greenland Ice Sheet surface mass balance variability, *Geophys. Res. Lett.*, *41*, 470–475, doi:10.1002/2013GL058172.
Gillet-Chaulet, F., O. Gagliardini, H. Seddik, M. Nodet, G. Durand, C. Ritz, T. Zwinger, R. Greve, and D. G. Vaughan (2012), Greenland Ice Sheet contribution to sea level rise from a new-generation ice sheet model, *Cryosphere*, *6*(6), 1561–1576, doi:10.5194/Tc-6-1561-2012.
Goelzer, H., P. Huybrechts, J. J. Furst, F. M. Nick, M. L. Andersen, T. L. Edwards, X. Fettweis, A. J. Payne, and S. Shannon (2013), Sensitivity of Greenland Ice Sheet projections to model formulations, *J. Glaciol.*, *59*(216), 733–749, doi:10.3189/2013jog12j182.
Greve, R. (1997), Application of a polythermal three-dimensional ice sheet model to the Greenland Ice Sheet: Response to steady state and transient climate scenarios, *J. Clim.*, *10*(5), 901–918, doi:10.1175/1520-0442.
Greve, R., and U. C. Herzfeld (2013), Resolution of ice streams and outlet glaciers in large-scale simulations of the Greenland Ice Sheet, *Ann. Glaciol.*, *54*(63), 209–220, doi:10.3189/2013aog63a085.
Greve, R., F. Saito, and A. Abe-Ouchi (2011), Initial results of the SeaRISE numerical experiments with the models SICOPOLIS and IcIES for the Greenland Ice Sheet, *Ann. Glaciol.*, *52*(58), 23–30.
Hanna, E., et al. (2013), Ice sheet mass balance and climate change, *Nature*, *498*(7452), 51–59, doi:10.1038/Nature12238.
Helsen, M. M., R. S. W. van de Wal, M. R. van den Broeke, W. J. van de Berg, and J. Oerlemans (2012), Coupling of climate models and ice sheet models by surface mass balance gradients: Application to the Greenland Ice Sheet, *Cryosphere*, *6*(2), 255–272, doi:10.5194/Tc-6-255-2012.
Huybrechts, P., and J. de Wolde (1999), The dynamic response of the Greenland and Antarctic Ice Sheets to multiple-century climatic warming, *J. Clim.*, *12*(8), 2169–2188, doi:10.1175/1520-0442.
Johnsen, S. J., et al. (1997), The delta O-18 record along the Greenland Ice Core Project deep ice core and the problem of possible Eemian climatic instability, *J. Geophys. Res.*, *102*(C12), 26,397–26,410, doi:10.1029/97JC00167.
Joughin, I., R. B. Alley, and D. M. Holland (2012), Ice sheet response to oceanic forcing, *Science*, *338*(6111), 1172–1176, doi:10.1126/Science.1226481.
Le Meur, E., and P. Huybrechts (1998), Present-day uplift patterns over Greenland from a coupled ice sheet/visco-elastic bedrock model, *Geophys. Res. Lett.*, *25*(21), 3951–3954, doi:10.1029/1998GL900052.
Lipscomb, W., J. Fyke, M. Vizcaino, W. Sacks, J. Wolfe, M. Vertenstein, A. Craig, E. Kluzek, and D. Lawrence (2013), Implementation and initial evaluation of the Glimmer Community Ice Sheet Model in the Community Earth System Model, *J. Clim.*, *26*(19), 7352–7371, doi:10.1175/JCLI-D-12-00557.1.
Meure, C. M., D. Etheridge, C. Trudinger, P. Steele, R. Langenfelds, T. van Ommen, A. Smith, and J. Elkins (2006), Law Dome $CO_2$, $CH_4$ and $N_2O$ ice core records extended to 2000 years B.P, *Geophys. Res. Lett.*, *33*, L14810, doi:10.1029/2006GL026152.
Mikolajewicz, U., M. Groeger, E. Maier-Reimer, G. Schurgers, M. Vizcaino, and A. M. E. Winguth (2007a), Long-term effects of anthropogenic $CO_2$ emissions simulated with a complex Earth system model, *Clim. Dyn.*, *28*(6), 599–631, doi:10.1007/s00382-006-0204-y.
Mikolajewicz, U., M. Vizcaino, J. Jungclaus, and G. Schurgers (2007b), Effect of ice sheet interactions in anthropogenic climate change simulations, *Geophys. Res. Lett.*, *34*, L18706, doi:10.1029/2007GL031173.
Moon, T., I. Joughin, B. Smith, and I. Howat (2012), 21st century evolution of Greenland outlet glacier velocities, *Science*, *336*(6081), 576–578, doi:10.1126/science.1219985.
Nick, F. M., A. Vieli, M. L. Andersen, I. Joughin, A. Payne, T. L. Edwards, F. Pattyn, and R. S. W. van de Wal (2013), Future sea level rise from Greenland's main outlet glaciers in a warming climate, *Nature*, *497*(7448), 235–238, doi:10.1038/Nature12068.
Price, S. F., A. J. Payne, I. M. Howat, and B. E. Smith (2011), Committed sea level rise for the next century from Greenland Ice Sheet dynamics during the past decade, *Proc. Natl. Acad. Sci. U.S.A.*, *108*(22), 8978–8983, doi:10.1073/Pnas.1017313108.
Rae, J. G. L., et al. (2012), Greenland Ice Sheet surface mass balance: Evaluating simulations and making projections with regional climate models, *Cryosphere*, *6*(6), 1275–1294, doi:10.5194/Tc-6-1275-2012.
Reeh, N. (1991), Parameterization of melt rate and surface temperature on the Greenland Ice Sheet, *Polarforschung*, *59*(3), 113–128.
Ridley, J. K., P. Huybrechts, J. M. Gregory, and J. A. Lowe (2005), Elimination of the Greenland Ice Sheet in a high $CO_2$ climate, *J. Clim.*, *18*(17), 3409–3427, doi:10.1175/Jcli3482.1.
Rignot, E., I. Velicogna, M. R. van den Broeke, A. Monaghan, and J. Lenaerts (2011), Acceleration of the contribution of the Greenland and Antarctic Ice Sheets to sea level rise, *Geophys. Res. Lett.*, *38*, L05503, doi:10.1029/2011GL046583.
Robinson, A., R. Calov, and A. Ganopolski (2011), Greenland Ice Sheet model parameters constrained using simulations of the Eemian interglacial, *Clim. Past*, *7*(2), 381–396, doi:10.5194/Cp-7-381-2011.
Schoof, C., and I. Hewitt (2013), Ice sheet dynamics, *Annu. Rev. Fluid Mech.*, *45*, 217–239, doi:10.1146/Annurev-Fluid-011212-140632.
Shepherd, A., et al. (2012), A reconciled estimate of ice sheet mass balance, *Science*, *338*(6111), 1183–1189, doi:10.1126/science.1228102.
van Angelen, J. H., J. T. M. Lenaerts, S. Lhermitte, X. Fettweis, P. K. Munneke, M. R. van den Broeke, E. van Meijgaard, and C. J. P. P. Smeets (2012), Sensitivity of Greenland Ice Sheet surface mass balance to surface albedo parameterization: A study with a regional climate model, *Cryosphere*, *6*(5), 1175–1186, doi:10.5194/Tc-6-1175-2012.
van Vuuren, D. P., et al. (2011), The representative concentration pathways: An overview, *Clim. Change*, *109*(1–2), 5–31, doi:10.1007/S10584-011-0148-Z.
Vizcaino, M. (2014), Ice sheets as interactive components of Earth System Models: Progress and challenges, *Wires Clim. Change*, *5*(4), 557–568, doi:10.1002/Wcc.285.
Vizcaino, M., U. Mikolajewicz, M. Groeger, E. Maier-Reimer, G. Schurgers, and A. M. E. Winguth (2008), Long-term ice sheet-climate interactions under anthropogenic greenhouse forcing simulated with a complex Earth System Model, *Clim. Dyn.*, *31*(6), 665–690, doi:10.1007/s00382-008-0369-7.

Vizcaíno, M., U. Mikolajewicz, J. Jungclaus, and G. Schurgers (2010), Climate modification by future ice sheet changes and consequences for ice sheet mass balance, *Clim. Dyn.*, *34*(2–3), 301–324, doi:10.1007/S00382-009-0591-Y.

Vizcaino, M., W. H. Lipscomb, W. J. Sacks, and M. van den Broeke (2013), Greenland surface mass balance as simulated by the Community Earth System Model. Part II: 21st century changes, *J. Clim.*, *27*, 215–226, doi:10.1175/jcli-d-12-00588.1.

Widmann, M. (2009), Paleoclimate delayed Holocene warming, *Nat. Geosci.*, *2*(6), 380–381, doi:10.1038/Ngeo536.

Wouters, B., J. L. Bamber, M. R. van den Broeke, J. T. M. Lenaerts, and I. Sasgen (2013), Limits in detecting acceleration of ice sheet mass loss due to climate variability, *Nat. Geosci.*, *6*(8), 613–616, doi:10.1038/ngeo1874.

Ziemen, F. A., C. B. Rodehacke, and U. Mikolajewicz (2014), Coupled ice sheet–climate modeling under glacial and preindustrial boundary conditions, *Clim. Past*, *10*(5), 1817–1836, doi:10.5194/cp-10-1817-2014.